Reference: *Biol. Bull.* **181:** 408–418. (December, 1991)

Spatial Information in the Three-Dimensional Fine Structure of an Aquatic Odor Plume

PAUL A. MOORE* AND JELLE ATEMA

Boston University Marine Program, Marine Biological Laboratory, Woods Hole, Massachusetts 02543

Abstract. Turbulent odor plumes play an important role in many chemically mediated behaviors, yet the fine scale spatial structure of plumes has not been measured in detail. With the use of a newly introduced microelectrochemical recording technique, we have measured, in some detail, the fine structure of an aquatic odor plume in the laboratory. We sampled a turbulent odor plume at 10 Hz with a spatial sampling area of 0.02 mm^2, approximately that of a chemoreceptor sensillum of the lobster, *Homarus americanus*. A 3-min record was sampled at 63 different sites in 3 dimensions (x, y, z). As expected from time averaging models, the mean values of pulse parameters such as height and onset slope were greatest near the source. However, what cannot be described by time averaging models is the instantaneous distribution of pulses: periodically high peaks with steep concentration slopes (well above the local average and far above predictions from averaging models) can be found far away from the source. However, the probability of above-average pulse heights decreases with distance from the source in x, y, and z directions. The most intense odor fluctuations occurred along the x axis (the cross-sectional center of the plume). Odor profiles were analyzed with three different models of sensory filters; logarithmic, probability, and temporal filters. This analysis indicates that features contained within the plume structure could be used as directional cues for orienting animals. It remains to be demonstrated that animals use such sensory filters to extract biologically relevant spatial information from odor plumes.

Received 14 December 1990; accepted 5 August 1991.

* Present address and correspondence: Department of Pharmacology, Campus box C236, University of Colorado Health Science Center, 4200 East Ninth Ave., Denver, CO 80262

Introduction

Many orientation studies have tried to elucidate the role of chemical signals in initiating and controlling orientation of an organism to an odor source. Authors have not only debated the behavioral mechanisms involved in chemically mediated orientation [Bell and Cardé, 1984 (preface); Bell, 1984; Kennedy, 1986], but also whether the odor signal plays a role in directional information (Preiss and Kramer, 1986; Sanders, 1986). Terms such as chemotaxis, klinokinesis, and menotaxis (Fraenkel and Gunn, 1961) have been tied to behavioral outputs of orienting animals, with a variety of underlying assumptions of the odor patterns and distributions as inputs. Yet in all of these studies, biologically relevant quantification of the stimulus signal either in the behavioral testing arena or arriving at the chemoreceptor organ has not been undertaken.

For years, orientation studies assumed that odor dispersion could be effectively described by time-averaged or Gaussian distribution models (Sutton, 1953; Bossert and Wilson, 1963). This model works for those organisms that operate either at small spatial scales *i.e.,* bacteria (Berg and Purcell, 1977), or sample over long time intervals *i.e.,* tsetse flies (Bursell, 1984). For animals that operate at other time and space scales, this model is a poor predictor of animal behavior (Elkinton *et al.,* 1984). Murlis and Jones (1981) and Atema (1985) have shown that odor distributions are quite heterogeneous as compared to the time-averaged models.

Still, quantification of odor signals at behaviorally relevant time and space scales remains rare (Murlis, 1986; Moore and Atema, 1988a). Present aerial studies use techniques such as smoke trails and bubble machines to try and quantify odor dispersal (David *et al.,* 1982; Brady *et al.,* 1989). These techniques only give qualitative de-

scriptions of wind patterns. They do not give quantitative data on odor signals within or around the smoke patches or soap bubbles. The few studies that have quantified odor dispersal patterns have sampled relatively few sites (Murlis, 1986; Murlis and Jones, 1981), and the ion detectors used in these studies have a larger sampling volume than that of a biologically relevant sampling device, *e.g.*, an insect antenna. Aquatic studies have used sensors with greater spatial resolution than those used in aerial studies, but thus far, like terrestrial studies, these studies have only sampled a few points down current from the odor source (Atema, 1985; Moore and Atema, 1988a; Zimmer-Faust *et al.*, 1988). In addition, these studies involve techniques that may not sample at spatial scales relevant to animal chemosensory detectors (See Moore *et al.*, 1989, for discussion). Finally, to the best of our knowledge, we know of no study that has quantified odor signals outside the cross-sectional center of the plume.

Fluid dynamic principles apply equally in air and water; the difference can be bridged with a simple scaling factor (Vogel, 1981). The diffusion of a chemical tracer will be different in the two mediums, which will cause slight differences in the fine scale structure of odor plumes in air *versus* water. However, the aquatic environment provides an easier medium in which to measure and model odor distributions for a variety of reasons. The space scales in an aquatic environment are much smaller, which allows for easier physical modelling of plumes. With the introduction of microelectrochemical measurement techniques to chemoreception sciences (Moore *et al.*, 1989), quantification of stimulus concentrations under biologically relevant time and space scales and direct measurement of boundary layers are possible. Additionally, diffusion calculations and measurements are easier in water because there is no partitioning of stimulus molecules at air-water interfaces and there are no mucus layers surrounding the sensory surfaces of aquatic chemoreceptors. The compounds for which electrochemical techniques have been perfected (dopamine, serotonin, *etc.*) have approximately the same molecular weight as many of the stimulatory compounds for aquatic animals (*e.g.*, amino acids, amines). Thus, they have similar diffusion properties. Since the only difference between the physical dynamics of turbulent dispersal in water and air are time and space scale differences, the results obtained in an aquatic medium are directly applicable to terrestrial environments. Turbulence will vary depending on the environmental conditions. Different conditions will lead to different parameter values.

Our study was designed to describe quantitatively an aquatic odor plume at both the spatial and temporal sampling scales of the lobster, *Homarus americanus*. This animal samples chemical signals with a variety of receptor organs. For orientation behavior it depends largely upon sensory input from the lateral antennules (Devine and Atema, 1982). These antennules contain dense rows of cylindrical aesthetasc hairs, which hold the dendrites of primary chemoreceptor cells. Each hair is .03 mm in diameter at the tip and 1 mm in length. The distal 0.8 mm of cuticle surrounding the hair is thought to be completely permeable to odor molecules (Ghiradella *et al.*, 1968). Thus, it is likely that the aesthetasc hair can sample odor over the entire distal surface area of the cylinder. To measure at the space scales relevant to this lobster receptor organ, one needs a device with similar spatial dimensions as the aesthetasc sensillum, so that fluid boundary layers, and thus odor diffusion, will be similar. To accomplish this, electrochemical electrodes with 100–150 μm diameters were chosen to model the spatial scales and fluid dynamics of a single aesthetasc hair.

Just as important as matching the spatial resolution of receptor cells and electrodes is the matching of their temporal resolution. We define the temporal sampling rate of a chemoreceptor cell as the inverse of the integration period of the receptor. This is a specific period of time over which stimulus-generated cellular processes, including receptor-ligand binding, second messenger, and generator potentials events, are summed into a discrete receptor cell response. In realistic terms, there is probably no simple integration time of a receptor cell. Instead, it is a dynamic balance between the cell excitation and adaptation processes. However, for receptor modelling and signal analysis needs, an integration time must be estimated. Unfortunately, temporal sampling rates of chemoreceptor cells and organs are poorly understood. Consequently, estimates of receptor integration times must be drawn from the small amount of neurophysiological work involving flicker fusion frequency and receptor adaptation. Christensen and Hildebrand (1988) found CNS neurons and Kaissling *et al.* (1987) found peripheral receptors in two different moth species that give distinct responses to 10 Hz odor pulses. Similar studies in aquatic animals produced similar results (Marschall and Ache, 1989). Antennule receptor cells of *H. americanus* begin to adapt in 500 ms (Voigt and Atema, 1990) regardless of pulse length. Also, the downstroke of the antennule, when odor is sampled, takes about 100 ms (Moore and Atema, 1988a; unpubl. video analysis). Based on these results, we feel that an integration time is somewhere between 100 and 500 ms. Therefore, a temporal sampling of 10 Hz in an aquatic medium can give biologically relevant resolution of chemical signals.

Materials and Methods

Plume measurements

All measurements were taken in a flow-through flume (250 × 90 × 20 cm). Water depth varied from 19 cm at

the front to 21 cm at the rear due to an intentional downward tilt of the flume. Unfiltered seawater entered through 15 holes at the head of the tank. Sheets of fluorescent light grating ("egg crates," 8 mm^2 holes) wrapped with plastic screens (1.5 mm^2 mesh) served as collimators (four upstream, one downstream). The carrier flow rate was 1.8 ± .11/s (S.D., n = 10). Average flow velocity in the tank was 1.00 ± .06 cm/s (n = 10). The test solution (described below) was gravity fed through a 1 mm pasteur pipette at a rate of 50 ± 2 ml/min (n = 10). The nozzle of the pipette was placed in the cross-sectional center of the tank 9 cm off the bottom, roughly at the odor sampling plane of a 0.5 kg lobster. As a frame of reference for further plume descriptions, the source is at x, y, z = 0. The x-axis is the main axis of the plume, and the y-axis is the other horizontal axis. Initial observations of the fluid flow with red dye did not indicate any large asymmetries in the general flow. Red dye was also used in the test solution, and observations showed that the plume was neutrally buoyant with respect to the carrier flow.

A total of 63 different sampling sites were chosen in three dimensions (Fig. 1). Sites along the x-axis were 25, 50, and 100 cm from the source. Sites along the y-axis were −10, −5, 0, +5, +10 cm at all x-axis locations. In addition, at x = 50 cm we added y = ±20 cm and at x = 100 cm, y = ±20 and ±30 cm. Sites along the z-axis were 3, 9, 15 cm from the flume bottom, *i.e.*, −6 cm (below) and +6 cm (above) all x, y sites in the z = 0 plane. All sites were sampled sequentially, each for a 3-min period.

Electrochemical microelectrodes

The electrochemical electrodes used in these experiments were scaled to be within the spatial sampling range

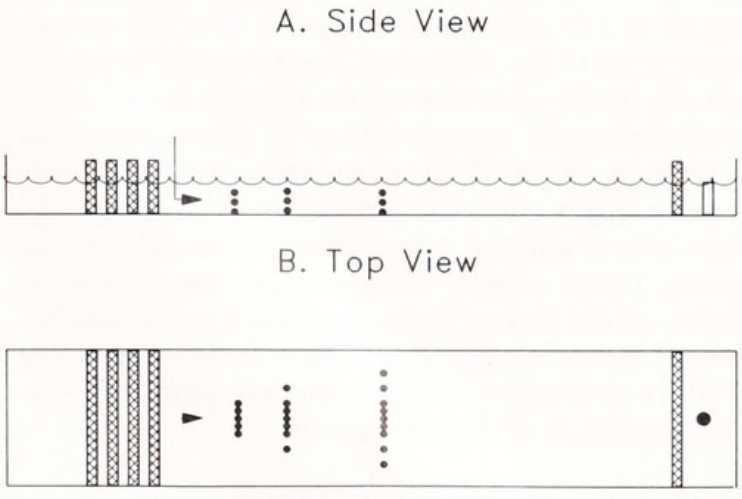

Figure 1. Diagram of flow-through flume used to create the turbulent odor plume. A: Side view, B: Top view. Flow from left to right. Arrow: odor tracer source. Dots: sampling sites. Hatched bars: collimators. Drain at far right. Scalloped water surface is merely symbolic and not reflecting degree of turbulence. See text for details.

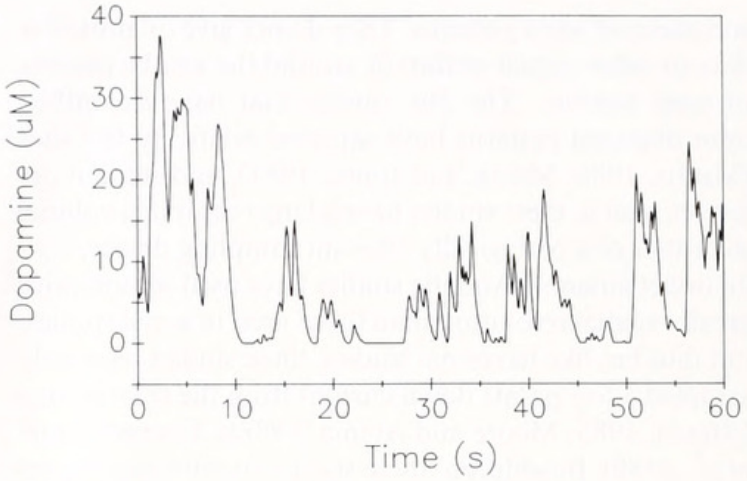

Figure 2. One-minute temporal profile of dopamine concentrations recorded at a 10 Hz sampling rate. This sampling site is at x = 25, y = z = 0. Source concentration is 2 m*M* dopamine.

of the olfactory sensilla of a macroscopic aquatic animal, specifically *Homarus americanus*. We used the graphite-epoxy capillary type of electrode (Gerhardt *et al.*, 1984) with a tip diameter of 100–150 μm. The sampling area is determined by the exposed carbon epoxy surface area. An electrode with a .15 mm diameter tip has an exposed surface area of .02 mm^2 (surface area of a circle = πr^2). A single aesthetasc hair has a sampling area of .06 mm^2 including the top and shaft (surface area of a cylinder plus circle = $2\pi rh + \pi r^2$). Thus, the sampling area of the electrodes used in this study is similar to that of a single aesthetasc hair. Recordings were made at a sampling rate of 10 Hz using the IVEC-5 (In Vivo Electrochemistry Computer System; Medical Systems Corp.). Each 100 ms epoch for the 10 Hz sampling rate is composed of a 50 ms epoch at 0.55 v (oxidation) followed by a 50 ms epoch at 0.0 v (reduction). The recording electrodes were sampled every 50 ms: analog-to-digital conversions of the samples occurred at 1 KHz, and data were averaged for the 50 ms time epoch. Further details of recording and digitizing are explained elsewhere (Moore *et al.*, 1989). All electrodes were calibrated in solutions of dopamine prepared in raw seawater and exhibited excellent linearity over a concentration range of 0.5 to 500 micromolar. To account for effects of molecular diffusion from odor patches, we chose source concentrations similar to those relevant to aquatic animals, such as the lobster. Amino acid levels found in the tissues of lobster prey range from .02 to 90 m*M* (Carr and Derby, 1986). Thus we chose a source concentration of 2 m*M* dopamine (and 0.5 m*M* ascorbic acid as an antioxidant).

Definition of terms

Odor signals can be dissected into various components and these components may be called by different names

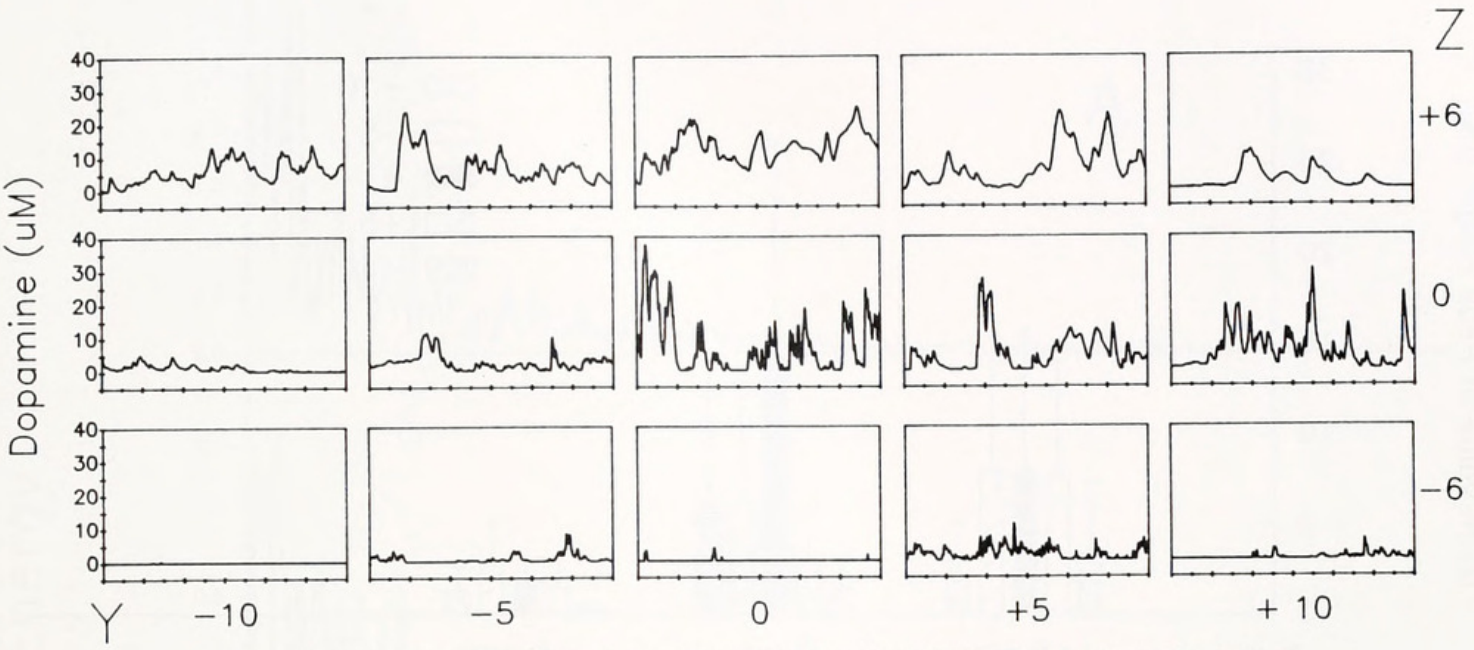

Figure 3. One-minute dopamine concentration profiles recorded at the x = 25 cm cross-sectional plane. One-minute segments were chosen to show the most intense period of odor fluctuations in the 3-min record. Numbers along bottom and right side indicate sampling site relative to source (x = y = z = 0). For example, the top left-hand graph labelled −10, +6 is 10 cm to the left and 6 cm up from the x-axis. Tick marks along the bottom indicate 5 s.

in the literature. Here we define the terms we will be using to describe an odor plume:

Odor profile: a concentration *versus* time plot that shows the concentration fluctuations at a single sampling site.

Odor burst: within an odor profile there are periods with and without odor. Periods during which the odor concentration is detectable by the sensor are called odor bursts. A burst ends when the concentration drops below detectable levels.

Off time: the period of time between two consecutive odor bursts.

Odor patch: the spatial equivalent of the odor burst. To a stationary sensor, a moving (spatial) patch of odor is measured as a (temporal) odor burst (Atema, 1987). With knowledge of the current speed, the size of the odor patch can be calculated from the length of the odor burst.

Odor pulse: within an odor burst, there may be multiple peaks and valleys of odor concentration. Each one of these peaks is considered a separate odor pulse only when the valley between the pulses falls to a value that is below 30% of the first pulse height. Odor pulses can be characterized by *pulse height,* highest concentration (measured against a background; see below) obtained during the pulse; *pulse length,* duration of pulse; *pulse onset slope,* maximum value of rising slope of pulse.

Data and statistical analysis

All measurements were converted from computer counts to micromolar concentrations of dopamine using the calibration factor determined for each electrode and set to a baseline of 0 dopamine (The theoretical detection limit of the system is below 10^{-9} *M* but due to electrical noise our limit is around 10^{-9} *M*). Concentration profiles plotted on a logarithmic scale had a baseline set at 10^{-8} *M*. This baseline roughly reflects both chemoreceptor cell thresholds commonly found in aquatic invertebrates (Ache, 1982) and amino acid background levels in seawater (Mopper and Lindroth, 1982; Carr, 1988). The natural chemical background of dopamine in seawater is not known, but unlikely to exceed 10^{-9} *M*.

Spectral analysis of the three-minute odor profiles were calculated via a Fast Fourier Transform method using a commercial signal processing program (DADiSP Worksheet). Fourier analysis breaks up a complex wave form into its component pure sine waves with different frequencies and amplitudes. This type of analysis gives a "power *versus* frequency" x, y plot, where frequency is expressed as cycles per second (as in a pure sine wave). In electrical terms, power is the integral of voltage squared over a given frequency range. Here, voltage reflects the pulse amplitude (*i.e.,* odor concentration) of a particular data point. Again in electrical terms, frequency is the inverse of the period of the different component sine waves of the signal being analyzed. In chemical terms, onset slopes are represented as frequencies: a steep slope with a short rise time is expressed in high frequency components. Thus, spectral analysis of an odor profile shows the mean value of pulse amplitudes within each frequency band. This is biologically relevant

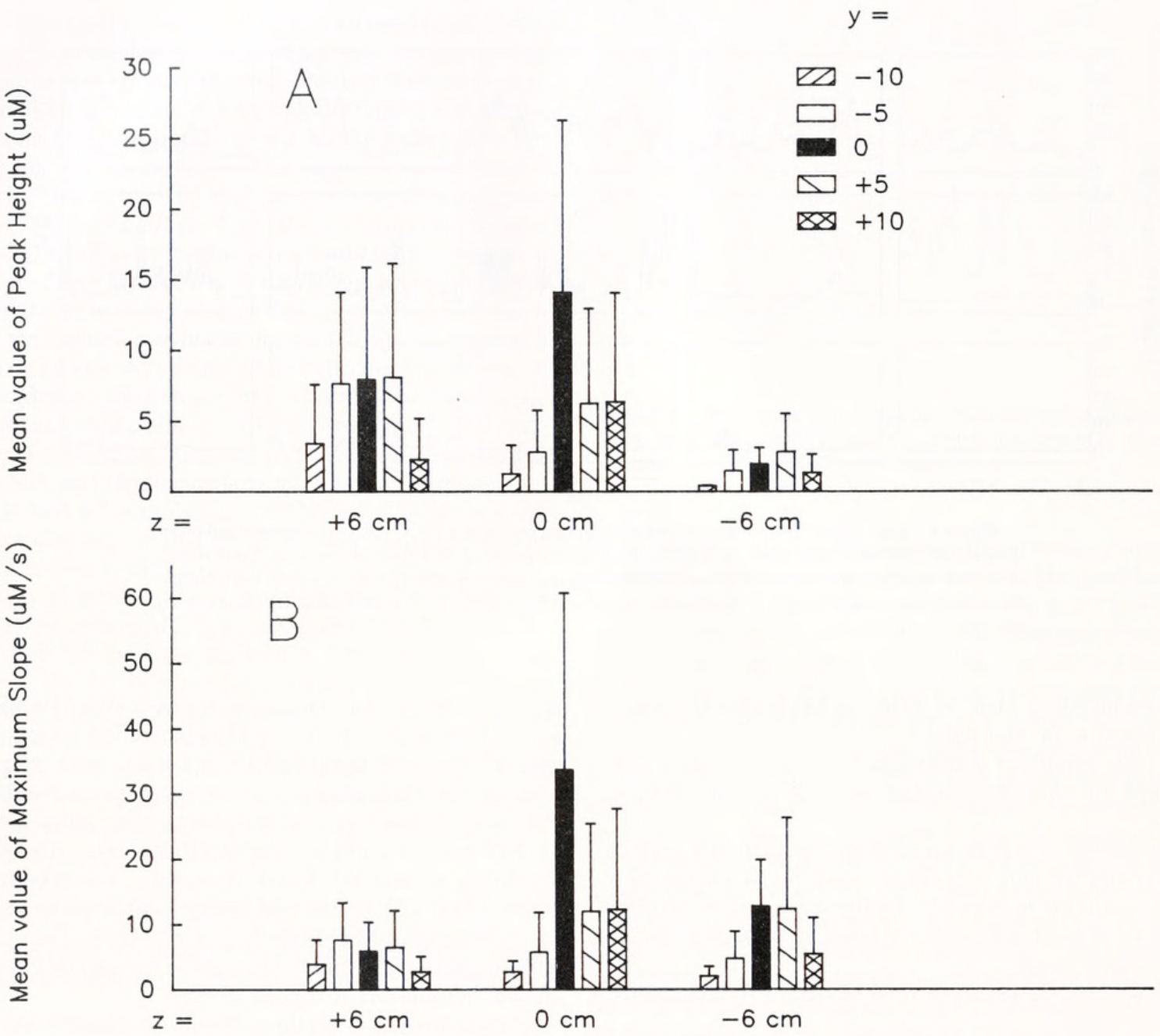

Figure 4. Mean (and standard deviation; T-bars) values of pulse height (A) and slope (B) for all pulses that occurred in the 3-min records at all x = 25 cm sites.

because it shows in which frequency band the strongest odor pulses lie.

Two odor profile characteristics, pulse height and maximum onset slope, were extracted from the calibrated odor plume signals based on the definitions above and the criteria set forth in Moore and Atema (1988a, b). The Tukey-Kramer multiple unplanned comparison method was used to compare the means for peak height and slope. These values, expressed in μM for pulse height and in μM/s for onset slope, were grouped into three log-step bins (.1–1, 1–10, 10–100). Although a small number of pulse height values were less than .1 μM, no pulse height values were higher than 100 μM. No slope values at any site were smaller than .1 μM/s or larger than 100 μM/s. For each site, probability distributions of height and slope for the three log-step bins were calculated from the number of occurrences within a log-step bin and the total number of pulses encountered at that site. The resulting values reflect the probability of encountering, at that site, a pulse having a height or slope value within a given bin.

Results

Odor profiles were characterized by bursts (Fig. 2). Bursts frequently lasted from 5 to 10 s, *e.g.*, Figure 2, 0–10 s or 38–45 s. Within a burst, pulses lasted between 0.5 and 6 s. Off times ranged from 0.2 to 3 s. The first odor burst in Figure 2 (0 to 10 s) shows four large (11, 38, 30,

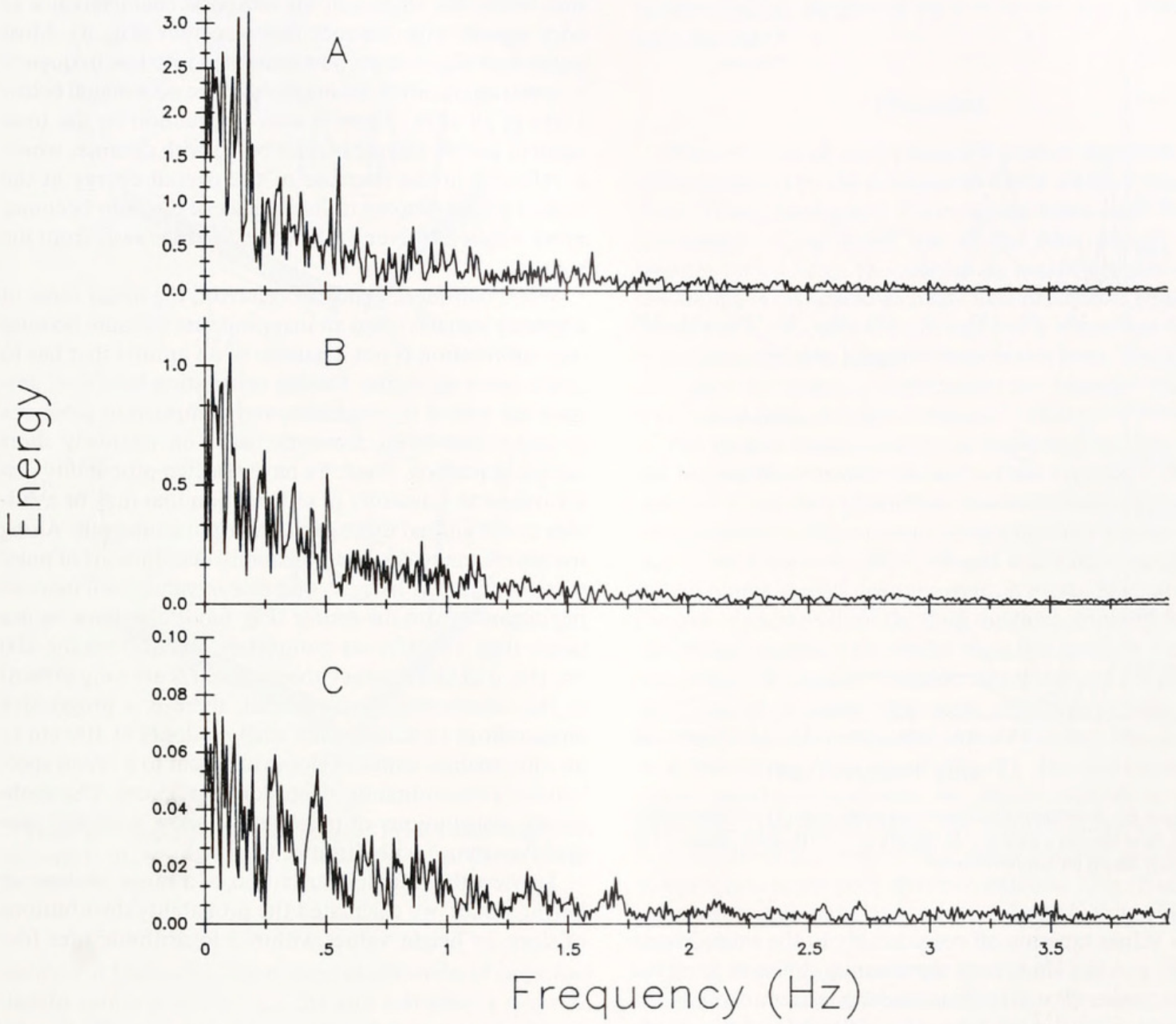

Figure 5. Frequency spectrum of concentration changes at three sites on the x-axis. A: x = 25, y = z = 0, B: x = 50, C: x = 100 cm. The ordinate is displayed as energy which corresponds to the number of pulses and pulse amplitude (See text). Note differences in Y-axis scaling. Based on 3-min records.

and 28 μM) and many smaller peaks. Using our definition, the first three peaks (11, 38 and 30 μM) are considered one pulse (because the value at valley is not less than 30% of the previous pulse amplitude, see Methods) and the last peak (28 μM) is considered a separate pulse. Note that peak concentrations are about 100 times diluted from source strength, *i.e.*, from 2 mM to 20 μM.

An initial qualitative picture of the spatial distribution of odor fluctuations is shown for the x = 25 plane in Figure 3. The most intense odor fluctuations occur in the center of the plume (site 25, 0, 0). At this site, large and rapid changes in concentration are more common than at other sites. Peak concentrations can exceed 25 μM dopamine. As areas further outside of this center point are sampled (y = ±5 and ±10 cm and z = ±6 cm), these large and sudden changes in concentration become less frequent. At one site (y = −10, z = −6), no odor could be detected. The z = +6 profiles (Fig. 3) contain large but considerably less steep steps in concentration but never exceed 25 μM dopamine. The z = −6 sites include small, but surprisingly steep, changes in concentration rarely exceeding 10 μM dopamine. Similar spatial distributions were seen in the x = 50 and x = 100 cm sampling planes (not shown for the sake of brevity).

Mean values of pulse height (Fig. 4a) and maximum slope (Fig. 4b) support the qualitative results seen in the 1-min profiles (Fig. 3). The highest values of both pulse height and slope are seen in the center of the odor plume,

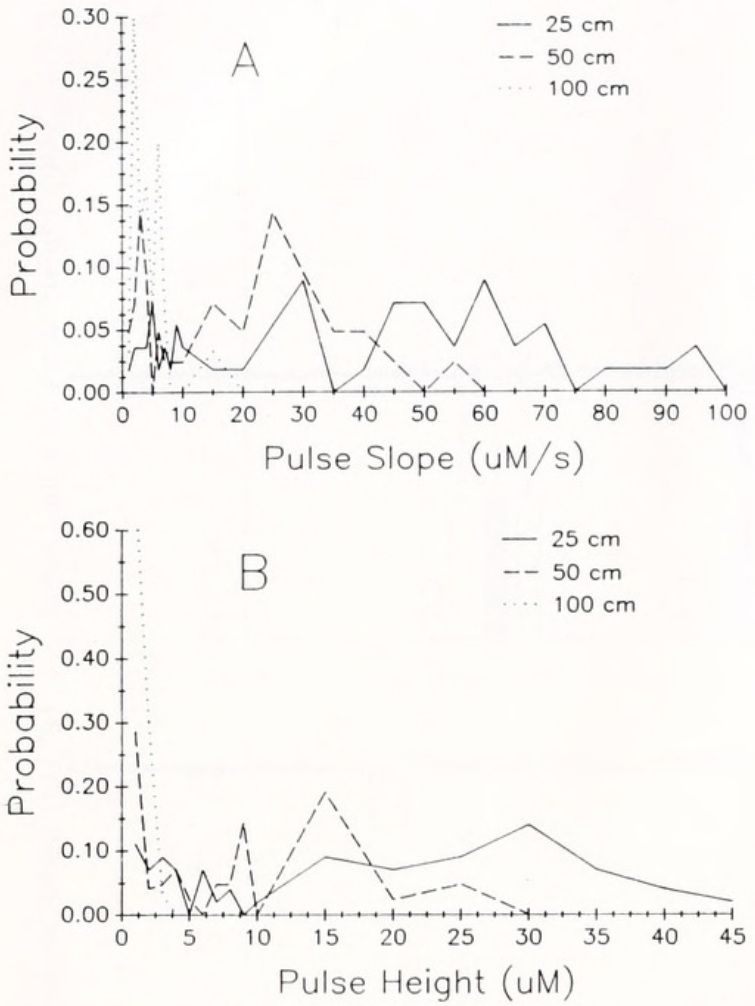

Figure 6. Probability distributions of pulse slope (A) and pulse height (B) at three sites on x-axis: x = 25 (Solid), x = 50 (Dashed), and x = 100 (Dotted). Based on 3-min records.

with values tapering off considerably to the sides. The (x = 25, y = 0) values were significantly different from the other means ($P < .01$). This tapering is asymmetrical: the differences in the left (y = −5, −10) and right (y = +5, +10) values within a z-plane are indicative of lateral meandering of the entire plume. The higher (z = +6) sampling sites had larger peak values (Fig. 4a) but slower-rising (Fig. 4b) odor pulses. The lower (z = −6) sampling sites had low intensity (Fig. 4a), but faster-rising (Fig. 4b) odor pulses; this will be discussed later. At the x = 50 and x = 100 cm sampling sites, the distributions of mean values were also centered around the cross-sectional middle of the plume with values tapering off (asymmetrically as above) away from the center. At all sites, the standard deviation of both pulse height and slope were approximately equal to the mean value at all sites. This is likely due to the chaotic nature of the turbulent odor plume and indicates that the mean value of any parameter is a poor indicator of the instantaneous value of that parameter.

Spectral analysis of the odor profiles (Fig. 5; note change in y-axis scale) from the three x-axis (z = y = 0) sampling sites shows the change in the temporal characteristics of odor signals with distance down-current (Fig. 4). Most pulses had slope values that translated into low frequency (<4 Hz) signals with the majority of the odor signal below 1 Hz at all sites. There is also a reduction in the total number and amplitude of odor bursts with distance, which is reflected in the decrease of the overall energy at the farther sites (compare ordinate scales): the odor becomes more widely and evenly distributed farther away from the source.

When considering animal behavior, the mean value of a sensory signal is often an inappropriate measure because this information is not available to an animal that has to make quick decisions. During orientation behavior, animals are forced by predation and competition pressures to make behavioral decisions based on relatively short sampling periods. Thus, we have selected probability distributions as a measure of information that may be available to the animal during short sampling intervals. Along the plume main axis, the probability distributions of pulse slopes shift to the left, *i.e.*, decrease in value, with increasing distance from the source (Fig. 6a). Pulse slope values larger than 15 μM/s are completely absent from the 100 cm site, and slope values above 55 μM/s are only present at the closest site. Thus, overall, there is a progressive change from predominantly shallow slopes at 100 cm to an intermediate range of slopes at 50 cm to a broad spectrum of predominantly steep slopes at 25 cm. The probability distributions of pulse height show a similar progressive change with distance (Fig. 6b).

To view the spatial distribution of a range of slope or height values, we calculated the probability distributions of slope or height values within 3 logarithmic bins (de-

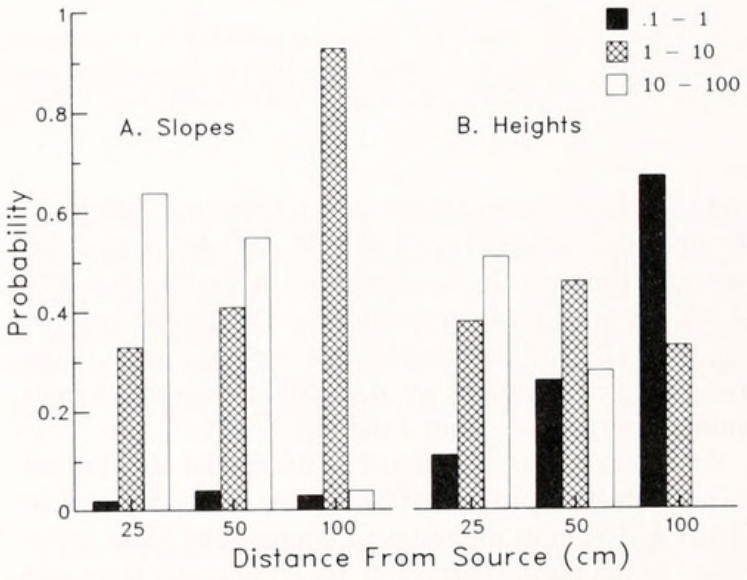

Figure 7. Probability distribution of pulse slope (A) and pulse height (B) at three sites on x-axis: x = 25, 50, 100. Probability values are calculated on the three bin sizes. .1–1, 1–10, 10–100.

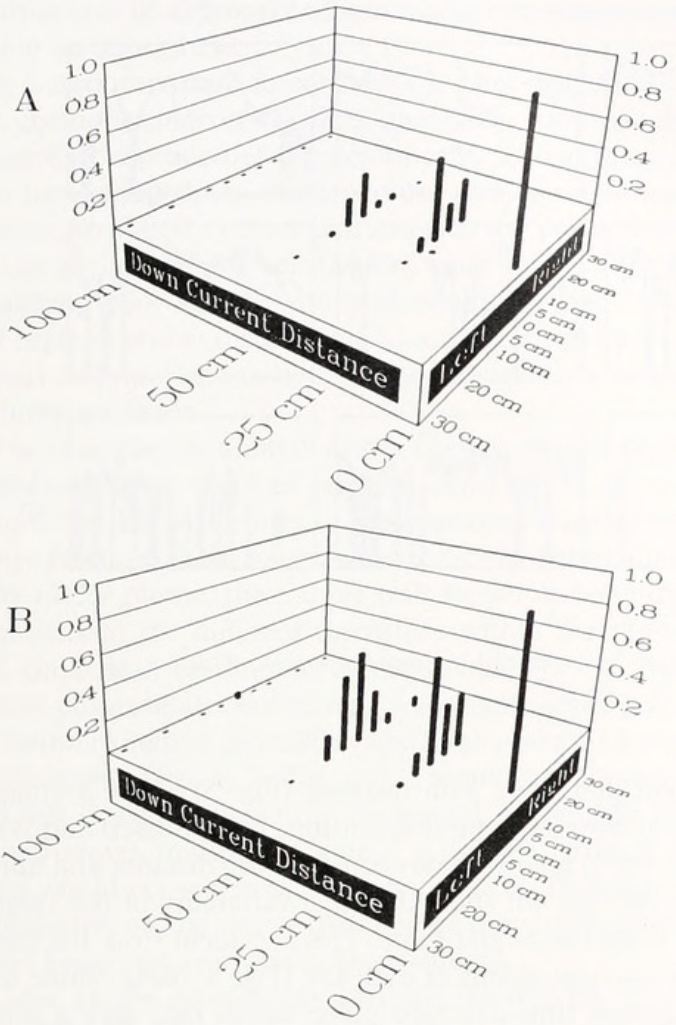

Figure 8. Spatial distribution of large (>10 μM) pulse heights (A) and large (>10 μM/s) pulse slopes (B) in the z = 0 plane. Source: $P = 1.0$ for reference.

scribed in Methods). The binned distribution of slope and height values at the x = 25, 50, and 100 sites (y = z = 0; Fig. 7) show a progressive change that was evident from continuous distributions in Figure 6. To illustrate how these probabilities are distributed in the x-y spatial plane, we plot one bin value at all of the sample points in this plane. The x-y spatial distribution of probabilities of large slopes (10–100 μM/s) in the z = 0 plane reveals that these values increase in the direction of the source (Fig. 8a). These values range from 0 (all x = 100 cm) to .64 (x = 25, y = 0 cm). At each x plane, the probabilities increase toward the middle of the plume with the largest values in the center. Similar distributions are seen in the z = +6 and z = −6 planes (not shown). The progressive changes seen in the slope distributions are also reflected in the pulse height distributions but with larger changes in the probabilities. The probabilities of large (10–100 μM) pulse heights in the z = 0 plane also increase toward the source and the center axis of the plume (Fig. 8b). The probabilities range from 0 at all but one of the x = 100 cm sites to .51 at the x = 25, y = 0 cm site. As with slopes, similar changes in probabilities are seen in the z = +6 and z = −6 planes (not shown).

Discussion

The structure of odor plumes is mainly due to turbulence produced by the mechanical forces within a moving fluid. These mechanical forces create large scale eddies (compared to the initial size of the odor plume) that transfer their energy to successively smaller eddies until the energy is dissipated as heat. This cascade of eddies is called the Kolmogoroff scale and has a lower size limit; molecular diffusion takes over below this limit. The lower size limit of eddies is determined by friction, viscous forces, and fluid velocity (Pedlosky, 1987).

The spatial range of eddies is important because it is the interaction between the size of the turbulent eddies and size of the odor plume that creates the size and length of concentration fluctuations within the odor plume (Aylor, 1976; Aylor *et al.*, 1976; Miksad and Kittredge, 1979). As the plume travels down-current, it expands relative to the size of eddies within the fluid medium. Initially, when the plume diameter is smaller than the smallest eddies, they cause the plume to meander as a whole. As the plume size expands to match the scale of eddies present, the plume is broken into separate patches of odor. This results in a fluctuating odor signal (Fig. 2). The final stage of plume growth occurs when the plume expands to sizes larger than the largest eddies. At this point, eddies begin to redistribute the odor within single patches and begin to homogenize the odor between patches. This results in signals that fluctuate less and have less off time (Fig. 3, top row).

Thus, as the plume as a whole and the patches within the plume increase in lifetime and size, there are changes taking place in the structure of the odor signal (Fig. 3).

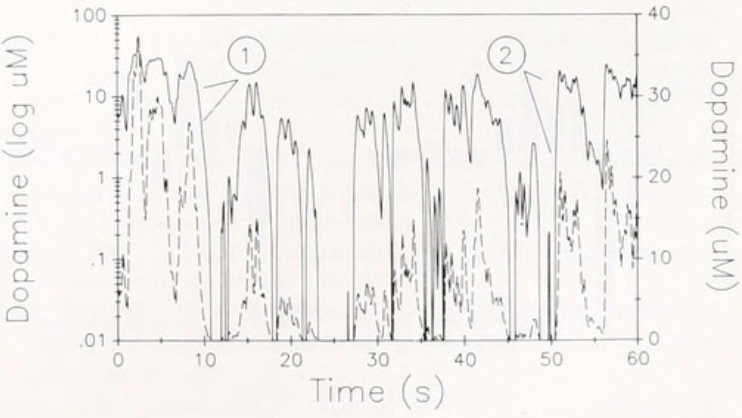

Figure 9. One-minute odor profiles from sample site at x = 25, y = z = 0 plotted on logarithmic (left hand, solid line) and linear (right hand, dashed line) scale. Dashed line is identical to profile in Figure 2. Baseline on logarithmic scale was set to 10^{-8} M (See text for explanation of 1 and 2).

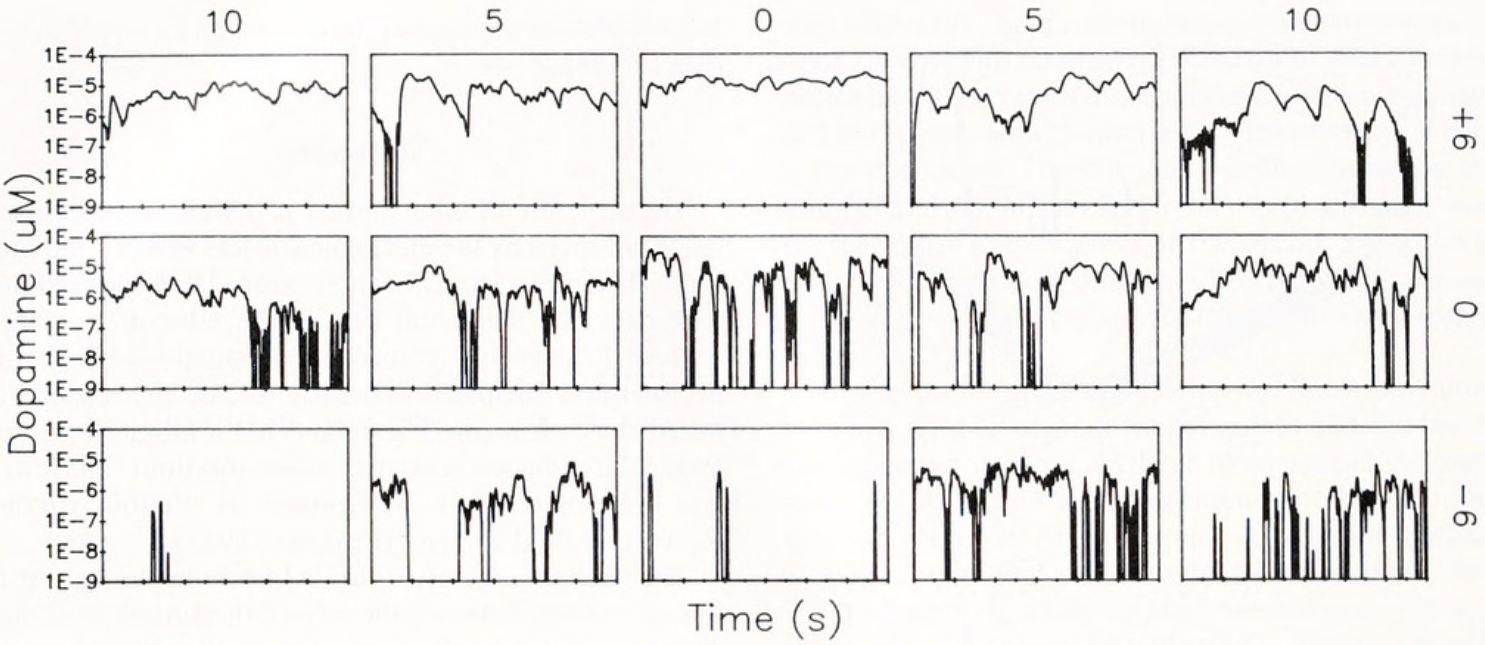

Figure 10. The same one-minute profiles shown in Figure 3 now plotted on logarithmic scale. Tick marks on bottom axis indicate 5 s.

The changes depend on the flow environment around the sampling point. The bottom row of profiles (Fig. 3) were sampled 3 cm from the bottom of the flume. The smooth, solid floor of the flume resulted in lower pulse heights but much faster rise times. Near the bottom of the flume, the eddies are confined to small and fast scales by the rigid, unmoving surface where fluid velocities must be zero. The top row of profiles (Fig. 3) were sampled 5 cm from the water surface. This moving surface allows larger and slower eddies, which acts as a "low pass" filter and dampens the faster rising slopes. This would result in an overall increased pulse height but slower rising slopes. These types of distributions are highly dependent upon the local substrate and fluid dynamic conditions.

These changes in the odor plume, with both distance and time can be seen as decreases in both mean pulse height and slope with distance (Fig. 5). Time-averaged plume dispersion models (Sutton, 1953; Bossert and Wilson, 1963) predict these decreases with distance and time, but they do not show the large variability of the values for pulse height and slope. This is evident from the large standard deviations at each site (Fig. 5, bars). While the long-term time-averaged pulse values may give a good prediction of the plume structure (and from that spatial position within a plume), the actual short-term (1–5 s) mean values of pulse height and slope may predict a different plume structure (and hence incorrect directional or positional information).

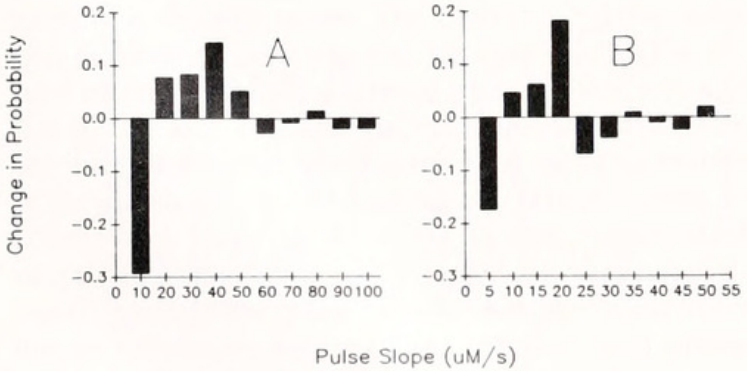

Figure 11. Probability distributions of pulse slope at the x = 25, y = z = 0 (A) and x = 50 (B) sampling sites. Solid bars represent change in distribution of same data as it is played through a model chemoreceptor filter (Moore and Atema, 1988; Model–Raw data). Positive values indicate enhancement from model, whereas negative values indicate reduction.

For an order of magnitude estimate, Atema (1988) reported that physiological responses of chemoreceptor cells may average over 0.01–1 s, and that behavioral responses may use sample intervals of 0.1–1000 s. Therefore, plume measurements averaging over periods longer than 1 s may be poor predictors of animal behavior within an odor plume. Ideally, one should measure an order of magnitude faster than the animal of study, *i.e.*, 1–100 ms resolution. For example, a behavioral assay with the gypsy moth produced quite different results than those that were predicted from time-averaged dispersion models (Elkinton *et al.*, 1984). Thus, it is not only important to consider both the spatial and temporal sampling scales of the chemoreceptor organ, but also the temporal scale of animal behavior analyzing odor concentrations. Probability distributions of parameters are a method to view the type of information available to the animal over a limited number of samples rather than the whole 3-min recordings. Animals may well base their behavioral decisions on sampling and encounter probabilities (Kamil, 1988). Therefore, probability

analysis may be appropriate for assessing orientation cues within an odor plume.

It is also important to consider the filter properties of the chemoreceptor cells when analyzing odor signals. Physiological properties of receptor cells, such as integration time, adaptation, disadaptation, and dose-response curves, can filter the odor signal and alter its "perception" by the chemoreceptor cell (Moore and Atema, 1988a). Analyzing odor signals with biologically realistic filters will begin to give us insights into how the CNS views odor signals and may lead to how behavioral decisions within a plume are made.

For example, an animal with a chemoreceptor organ containing three types of receptor cells (A, B, and C) "tuned" to different ranges of pulse heights or intensities (range fractionation). As the animal moves within a turbulent odor plume, these three cells would respond differentially at the different intensities within the plume and could lead the animal to the source. At the most distant points in an odor plume, where only small peaks are found in highest probability and large peaks are rarely encountered (Figs. 6, 7, 8b), cell A would fire the most and cell B would have only occasional output. As the animal moves toward the source, a different pattern of firing would occur across a cell population. Directional information on the source can then be derived from different firing patterns (across fiber pattern).

Odor plume profiles are normally plotted on linear scales (Murlis, 1986; Moore and Atema, 1988a), but chemoreceptor cells often have linear responses to logarithmic changes in concentrations. Plotting the x = 25, y = z = 0 odor profile (Fig. 2) on a log scale produces a quite different view of the odor signal fluctuations (Fig. 9). This type of filter (logarithmic) enhances concentration changes *between* odor bursts, but diminishes changes *within* the bursts. The two marks (# 1 and 2; Fig. 9) indicate nearly identical concentration changes on a linear scale, but the initial concentration change (#2) of an odor burst is much more prominent on the log scale than the concentration change within the odor burst (#1). These same changes are also seen in the cross-sectional view at the x = 25 cm sampling site (Fig. 10). Thus, the initial onset of the odor burst seems (on a log scale) to have the most dramatic concentration changes.

Chemoreceptor cells also have the temporally dynamic properties of adaptation and disadaptation that cause changes in the receptor cell output, response threshold, and dose-response functions (Borroni and Atema, 1988, 1989; Voigt and Atema, 1990). These two properties can function together to filter turbulent odor signals (Moore and Atema, 1988a, b). To examine how adaptation and disadaptation affect plume structure, we analyzed the x = 25, y = z = 0 sampling site with the 10 s temporal filter introduced in Moore and Atema (1988a). The 3 log scale (.1–1, 1–10, 10–100 μM) probability grouping performed on the data in this study was repeated on the filtered data. Figure 11 shows the changes in the probability distributions of the onset slopes from the raw data as it is filtered through the model. At both the x = 25 (Fig. 11a) and x = 50 (Fig. 11b) sites, the model enhances the probability of detecting slopes in the middle range of values. This temporally dynamic filter seems to eliminate the smaller amplitude, slower rising peaks that are evident within the raw data.

Within all of these different filtering methods, one common theme appears. Although turbulent odor plumes produce odor signals that seem random and chaotic, there are biological and computational methods of analysis that can track changes occurring within the structure of odor plumes. Which structural features are detectable and used by the animal for orienting within a turbulent plume? To answer this question, we must measure different turbulent odor signals at biologically relevant time and space scales and then analysis those results with biologically relevant spatial and temporal filters; *i.e.*, logarithmic, adaptation, and sampling behavior of the chemosensory organ.

Acknowledgments

The authors would like to thank Nat Scholz and Lynne Lacomis for assistance during measurements and reviewing an earlier version of this manuscript; Dr. Greg A. Gerhardt and Medical Systems for the generous support of equipment and technology; and Drs. Greg Gerhardt, Ring Cardé, and Fred Wasserman for critically reviewing this manuscript as a chapter in P.M.'s Ph.D. thesis. We would especially like to thank Dr. Keith Stolenzbach for discussion and development of some ideas presented in the discussion. This work supported by a grant from NSF (BNS 90-12952) to J. A. and a BUMP Alumni research award to P.M.

Literature Cited

Ache, B. W. 1982. Chemoreception and thermoreception. Pp. 369–398 in *The Biology of Crustacea, Vol. 3. Neurobiology: Structure and Function,* H. L. Atwood and D. C. Sandeman, eds. Academic Press, NY.

Atema, J. 1988. Distribution of chemical stimuli. Pp. 29–56 in *Sensory Biology of Aquatic Animals,* J. Atema, A. N. Popper, R. R. Fay and W. N. Travolga, eds. Springer-Verlag, NY.

Atema, J. 1987. Chemoreceptor adaptation: a patch in space is a pulse in time. *Chem. Senses* **12:** 189–190.

Atema, J. 1985. Chemoreception in the sea: adaptation of chemoreceptors and behavior to aquatic stimulus conditions. *Soc. Exp. Biol. Symp.* **39:** 387–423.

Atema, J., K. Holland, and W. Ikehara. 1980. Olfactory responses of yellowfin tuna (*Thunnus albacares*) to prey odors: chemical search image. *J. Chem. Ecol.* **6:** 457–465.

Aylor, D., J-Y. Parlange, and J. Granett. 1976. Turbulent dispersion of disparlure in the forest and male gypsy moth response. *Env. Ent.* **10:** 211–218.

Aylor, D. E. 1976. Estimating peak concentrations of pheromones in the forest. Pp. 177–188 in *Perspectives in Forest Entomology,* J. E. Anderson and M. K. Kaya, eds. Academic Press, NY.

Bell, W. J. 1984. Chemo-orientation in walking insects. Pp. 93–106 in *Chemical Ecology of Insects,* W. J. Bell and R. T. Cardé, eds. Sinauer Associates, Inc., MA.

Bell, W. J., and R. T. Cardé (eds.). 1984. *Chemical Ecology of Insects,* Sinauer Associates, Inc., MA.

Berg, H. C., and E. M. Purcell. 1977. Physics of chemoreception. *Biophys. J.* **20:** 193–219.

Bossert, W. H., and E. O. Wilson. 1963. The analysis of olfactory communication among animals. *J. Theor. Biol.* **5:** 443–469.

Borroni, P. F., and J. Atema. 1989. Adaptation in chemoreceptor cells II. The effects of cross-adapting backgrounds depend on spectral tuning. *J. Comp. Physiol. A.* **165:** 669–677.

Borroni, P. F., and J. Atema. 1988. Adaptation in chemoreceptor cells I. Self-adapting backgrounds determine threshold and cause parallel shift of response function. *J. Comp. Physiol. A.* **164:** 67–74.

Brady, J., G. Gabriella, and M. J. Packer. 1989. Odour movement, wind direction, and the problem of host-finding by tsetse flies. *Physiol. Entomol.* **14:** 369–380.

Bursell, E. 1984. Observations on the orientation of tsetse flies (Glossina pallidipes) to wind-borne odours. *Physiol. Entomol.* **9:** 133–137.

Carr, W. E. S. 1988. The molecular nature of chemical stimuli in the aquatic environment. Pp. 3–28 in *Sensory Biology of Aquatic Animals,* J. Atema, A. N. Popper, R. R. Fay, and W. N. Travolga, eds. Springer-Verlag, NY.

Carr, W. E. S., and C. D. Derby. 1986. Behavioral chemoattractants for the shrimp, *Palaemonetes pugio:* identification of active components in food extracts and evidence of synergistic mixture interactions. *Chem. Senses* **11:** 49–64.

Christensen, T. A., and J. G. Hildebrand. 1988. Frequency coding by central olfactory neurons in the Sphinx moth *Manduca sexta. Chem. Senses* **13:** 123–130.

David, C. T., J. S. Kennedy, A. R. Ludlow, J. N. Perry, and C. Wall. 1982. A reappraisal of insect flight towards a distant, point source of wind-bourne odor. *J. Chem. Ecol.* **8:** 1207–1215.

Devine, D. V., and J. Atema. 1982. Function of chemoreceptor organs in spatial orientation of the lobster, *Homarus americanus:* differences and overlap. *Biol. Bull.* **163:** 144–153.

Elkinton, J. S., R. T. Cardé, and C. J. Mason. 1984. Evaluation of time-average dispersion models for estimating pheromone concentration in a deciduous forest. *J. Chem. Ecol.* **10:** 1081–1108.

Fraenkel, G. S., and D. L. Gunn. 1961. The orientation of animals. 2nd edition, Dover Publishers Inc., N.Y.

Gerhardt, G. A., A. F. Oke, G. Nagy, B. Moghaddam, and R. N. Adams. 1984. Nafion-coated electrodes with high selectivity for CNS electrochemistry. *Brain Research* **290:** 390–395.

Ghiradella, H., J. F. Case, and J. Cronshaw. 1968. Structure of aesthetascs in selected marine and terrestrial decapods: chemoreceptor morphology and environment. *Am. Zool.* **8:** 603–621.

Kaissling, K. E., C. Zack-Straussfeld, and E. Rumbo. 1987. Adaptation processes in insect olfactory receptors: mechanisms and behavioral significance. Pp. 104–112 in *Olfaction and Taste IX,* S. Roper and J. Atema, eds. N.Y. Acad. Sci.

Kamil, A. C. 1989. Behavioral ecology and sensory biology. Pp. 189–202 in *Sensory Biology of Aquatic Animals,* J. Atema, A. N. Popper, R. R. Fay, and W. N. Travolga, eds. Springer-Verlag, NY.

Kennedy, J. S. 1986. Some current issues in orientation to odour sources. Pp. 11–25 in *Mechanisms in Insect Olfaction,* T. L. Payne, M. C. Birch, and C. E. J. Kennedy, eds. Clarendon Press, NJ.

Marschall, H-P., and B. W. Ache. 1989. Response dynamics of lobster olfactory neurons during simulated natural sampling. *Chem. Senses* **14:** 725.

Miksad, R. W., and J. Kittredge. 1979. Pheromone aerial dispersion: a filament model. *14th Conf. Agric. and For. Met. Am. Met. Soc.* **1:** 238–243.

Moore, P. A., G. A. Gerhardt, and J. Atema. 1989. High resolution spatio-temporal analysis of aquatic chemical signals using microelectrochemical electrodes. *Chem. Senses* **14:** 829–840.

Moore, P. A., and J. Atema. 1988a. A model of a temporal filter in chemoreception to extract directional information from a turbulent odor plume. *Biol. Bull.* **174:** 355–363.

Moore, P. A., and J. Atema. 1988b. A mathematical computer model of the temporal filtering characteristics of chemosensory adaptation. *Chem. Senses* **13:** 722.

Mopper, K., and P. Lindroth. 1982. Diel and depth variations in dissolved free amino acids and ammonium in the Baltic Sea determined by shipboard HPLC analysis. *Limnol. Oceanogr.* **27:** 336–347.

Murlis, J. 1986. The structure of odour plume. Pp. 27–38 in *Mechanisms in Insect Olfaction,* T. L. Payne, M. C. Birch, and C. E. J. Kennedy, eds. Clarendon Press, NJ.

Murlis, J., and C. D. Jones. 1981. Fine-scale structure of odour plumes in relation to insect orientation to distant pheromone and other attractant sources. *Physiol. Entomol.* **6:** 71–86.

Pedlosky, J. 1987. *Geophysical Fluid Dynamics,* Springer-Verlag, NY.

Preiss, R., and E. Kramer. 1986. Pheromone-induced anemotaxis in simulated free flight. Pp. 6–80 in *Mechanisms in Insect Olfaction,* T. L. Payne, M. C. Birch, and C. E. J. Kennedy, eds. Claredon Press.

Sanders, C. J. 1986. The role of pheromone concentration in male moth flight behavior. Pp. 117–122 in *Mechanisms in Insect Olfaction,* T. L. Payne, M. C. Birch, and C. E. J. Kennedy, eds. Clarendon Press, NJ.

Sutton, O. G. 1953. *Micrometeorology,* McGraw-Hill, NY.

Vogel, S. 1981. *Life in Moving Fluids: the Physical Biology of Flow,* Princeton University Press, Princeton, NJ. 352 pp.

Voigt, R., and J. Atema. 1990. Adaptation in chemoreceptor cells. III. Effects of cumulative adaptation. *J. Comp. Physiol. A.* **166:** 865–874.

Zimmer-Faust, R. K., J. M. Stanfill, S. B. Collard III. 1988. A fast, multichannel fluorometer for investigating aquatic chemoreception and odor trails. *Limnol. Oceanogr.* **33:** 1586–1595.